Pertanika J. Sci. & Technol. 34 (5): 2597 - 2618 (2026)

PERTANIKA JOURNALS

SCIENCE & TECHNOLOGY

Journal homepage: http://www.pertanika.upm.edu.my/

Artificial Neural Network-Based UHF Partial Discharge Localisation in Mineral Oil with Datasets Based on TDOA

Zhi Yang Lim[1], Norhafiz Azis[1]*, Hafiz Rashidi Ramli[2], Mohd Amran Mohd Radzi[1], Nor Mohd Haziq Norsahperi[2], and Azrul Mohd Ariffin[3]

[1]Advanced Lightning, Power and Energy Research Centre (ALPER), Faculty of Engineering, Universiti Putra Malaysia, 43400 UPM Serdang, Selangor, Malaysia
[2]Department of Electrical and Electronic Engineering, Faculty of Engineering, Universiti Putra Malaysia, 43400 UPM Serdang, Selangor, Malaysia
[3]Department of Electrical and Electronics Engineering, College of Engineering, Institute of Power Engineering, Universiti Tenaga Nasional (UNITEN), Jalan IKRAM-UNITEN, 43000 Kajang, Selangor, Malaysia

ABSTRACT

This study presents a dataset generation procedure to train artificial neural networks (ANNs) for ultra-high frequency (UHF) partial discharge (PD) localisation in an oil-filled tank. The datasets were generated using the Time Difference of Arrival (TDOA) equations and augmented with samples containing random deviations. The PD localisation performance of the ANNs trained on the datasets was compared with that of the artificial bee colony (ABC), bat algorithm (BA), genetic algorithm (GA), particle swarm optimisation (PSO), and a non-iterative algorithm, based on the TDOAs of experimental UHF PD signals. An experiment was conducted in which UHF PD signals were captured with 4 patch-type wideband antennas and denoised using the variational mode decomposition (VMD) method. TDOAs were computed from both the original and denoised UHF PD signals through the First Peak Method (FPM) and Cumulative Energy Method (CEM). For the original UHF PD signals, the FPM produces TDOAs with lower mean absolute errors (MAEs) than the CEM. In contrast, the CEM produces TDOAs with lower MAEs than the FPM for the denoised UHF PD signals. TDOAs with lower MAEs generally lead to lower PD localisation errors. The trained ANNs consistently achieve the highest PD localisation accuracy, with average computation times ranging from 36.75 ms to 43.17 ms.

Keywords: Artificial neural network (ANN), mineral oil, partial discharge (PD) localisation, Time Difference of Arrival (TDOA), ultra-high frequency (UHF)

ARTICLE INFO

Article history:
Received: 22 May 2026
Accepted: 17 August 2026
Published: 30 October 2026

DOI: https://doi.org/10.47836/pjst.34.5.03

gs68246@student.upm.edu.my (Zhi Yang Lim)
norhafiz@upm.edu.my (Norhafiz Azis)
hrhr@upm.edu.my (Hafiz Rashidi Ramli)
amranmr@upm.edu.my (Mohd Amran Mohd Radzi)
nmhaziq@upm.edu.my (Nor Mohd Haziq Norsahperi)
Azrula@uniten.edu.my (Azrul Mohd Ariffin)
* Corresponding author

e-ISSN: 2231-8526

© Universiti Putra Malaysia Press

INTRODUCTION

The continuous operation of a power transformer relies on the integrity of its insulation system. Statistics indicate that insulation breakdown is a primary cause of transformer failures (Pattanadech & Muhr, 2016). Prolonged and unaddressed partial discharge (PD) within the insulation is a major contributor to such breakdowns (Chan et al., 2023). Therefore, PD diagnostics are among the most common techniques for monitoring transformer insulation condition and supporting predictive maintenance (AJ et al., 2018). An important aspect of PD diagnostics is the localisation of the PD sources within transformers (Zaki et al., 2020). This information can facilitate the formulation of targeted maintenance strategies for the transformers. Generally, PD localisation involves PD signal acquisition, PD signal denoising, Time Difference of Arrival (TDOA) computation, and application of the PD localisation algorithm (Desai & Sarathi, 2018).

The ultra-high frequency (UHF) method is a common technique for PD signal acquisition that detects electromagnetic signals emitted by PD sources in the frequency range of 0.3 to 3 GHz (Boya-Lara et al., 2022). The capability for online PD detection and source localisation represents a major advantage of the UHF method as compared with conventional electrical techniques based on IEC 60270 (Jahangir et al., 2017). Although transformer tanks function as a shield that increases the signal-to-noise ratio (SNR) of UHF PD signals (Jahangir et al., 2017), field measurements can still be affected by various types of noises, such as white noise, impulsive noise, and periodic narrowband interference (Boya-Lara et al., 2022). Therefore, effective denoising techniques are essential for improving the accuracy of the UHF method and minimising the risk of false diagnosis. Multivariate wavelet (MW) denoising, empirical mode decomposition (EMD), and variational mode decomposition (VMD) are common denoising methods for UHF PD signals (Long et al., 2021). Studies report that VMD can achieve better denoising performance at lower computational cost than EMD and wavelet-based methods (Long et al., 2021; Zhang et al., 2019).

Typical techniques for TDOA computation include the First Peak Method (FPM), Cumulative Energy Method (CEM), and Cross-Correlation Method (CCM). FPM determines the arrival time of a PD signal based on the first local peak whose absolute magnitude exceeds a predefined threshold (Hashim et al., 2023; Sinaga et al., 2012). In CEM, the arrival time of a PD signal is determined from the knee point of its cumulative energy curve (Kundu et al., 2009). For both the FPM and the CEM, TDOAs are calculated from the differences between the arrival times at 2 sensors. CCM computes the TDOA from the maximum point of the cross-correlation curve between 2 PD signals, assuming that signals from the same PD source share similar waveform patterns (Sinaga et al., 2012). Different TDOA computation methods may yield different TDOAs for the same PD signal (Kakeeto et al., 2008; Sinaga et al., 2012), and the performance of each method varies

across cases (Long et al., 2021). Since variations in TDOAs can affect the accuracy of PD localisation (Desai & Sarathi, 2018), the TDOA computation technique serves as a crucial factor in the overall PD localisation framework.

Over the years, research on TDOA-based PD localisation algorithms progresses from iterative approaches, such as the least-squares and Newton's algorithms, to optimisation algorithms such as the genetic algorithm (GA), particle swarm optimisation (PSO), and quantum genetic algorithm (QGA) (Lim et al., 2025). These optimisation algorithms do not require initial guesses and generally achieve higher localisation accuracy than the iterative approaches (Rathod et al., 2022). A non-iterative algorithm that provides faster estimation is also proposed by Kundu et al. (2009). To improve localisation accuracy, recent research explores the use of artificial intelligence (AI) techniques for PD localisation (Chan et al., 2023). For example, an artificial neural network (ANN) method is proposed by Taha et al. (2020) to determine optimal sensor placements on the transformer tank wall to enhance PD localisation accuracy. Hashim et al. (2023) investigate the application of ANN and adaptive neuro-fuzzy inference system (ANFIS) models for acoustic PD localisation. The study by Khodaveisi et al. (2024) evaluates several AI techniques, such as support vector machine (SVM) and backpropagation neural network (BPNN), for UHF PD localisation using a time-reversal approach.

For PD localisation, the performance of ANN depends on the training dataset. The datasets can be prepared from PD measurements conducted on the transformer (Hashim et al., 2023). However, this requires repeated on-site PD measurements (Zaki et al., 2020), and the actual PD location remains unknown unless the transformer tank is dismantled. These constraints might limit the size of the generated dataset, thereby affecting the performance of the trained ANNs (Basheer & Hajmeer, 2000). An alternative approach to dataset generation involves simulating PD signal propagation within the transformer tank, as demonstrated by Khodaveisi et al. (2024). This approach demands considerable time, and access to in-service transformer parameters is sometimes restricted (Chan et al., 2023). Therefore, this study adopts a different method for dataset generation, in which dataset samples are computed using the TDOA equations. This method avoids the need for large-scale on-site PD data collection and requires less time than the simulation-based approach. TDOA samples with random deviations are included to augment the datasets, as practical TDOAs often differ from the theoretical TDOAs due to various intricate factors, such as the complex propagation paths within the transformer tank and noise at the measurement sites (Ghosh et al., 2017; Jangjoo et al., 2023). The objective of this study is to examine the UHF PD localisation performance of ANNs trained on datasets generated by the proposed method. An experiment is conducted with a steel tank filled with mineral oil. UHF PD signals are acquired at 2 distinct PD locations within the tank, and the VMD method is applied to denoise the signals. The FPM and CEM are employed to compute

the TDOAs from both the original and denoised UHF PD signals. PD localisation is then performed using the computed TDOAs. The localisation performance of the trained ANNs is compared with the artificial bee colony (ABC), bat algorithm (BA), genetic algorithm (GA), particle swarm optimisation (PSO), and a non-iterative algorithm in terms of distance error and computation time.

METHODOLOGY

Mathematical Model of TDOA-Based PD Localisation

The test tank used in this study measured 1.00 m in length, 0.30 m in width, and 0.25 m in height, as shown in Figure 1. A 3-dimensional (3D) coordinate system was defined for the test tank, with the lower-left corner at the back set as the origin, O (0, 0, 0). The coordinates of the 4 UHF sensors were denoted as (x_1, y_1, z_1), (x_2, y_2, z_2), (x_3, y_3, z_3), and (x_4, y_4, z_4), while the PD source location was represented by (x, y, z). Based on this setup, the TDOA-based PD localisation model employed in this study was mathematically described by Equations 1-4 (Chan et al., 2023; Desai & Sarathi, 2018). In these equations, v refers to the propagation velocity of UHF signals in mineral oil, which is 2×10^8 m/s (CIGRE Working Group D1.29, 2017; Sinaga et al., 2012). The term T_1 denotes the time of arrival (TOA) of the UHF PD signal at UHF Sensor 1 (S_1), which served as the reference sensor. The TDOAs, τ_{21}, τ_{31}, and τ_{41}, were computed as the differences between the TOAs at UHF Sensors 2, 3 and 4, and the TOA at the reference sensor.

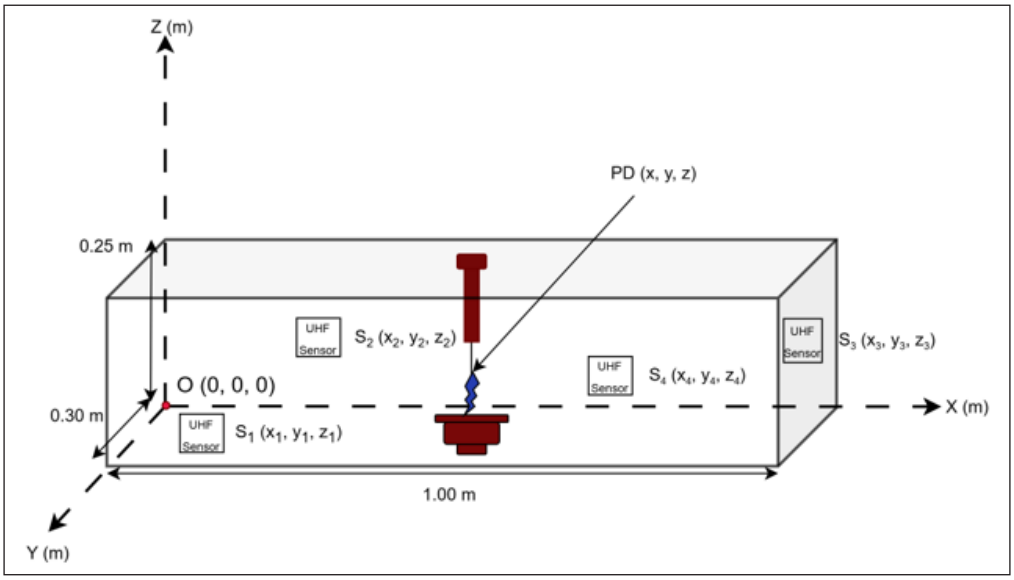

Figure 1. The test tank and the adopted 3D coordinate system

$$(x - x_1)^2 + (y - y_1)^2 + (z - z_1)^2 = (v \times T_1)^2 \quad [1]$$

$$(x - x_2)^2 + (y - y_2)^2 + (z - z_2)^2 = [v \times (T_1 + \tau_{21})]^2 \quad [2]$$

$$(x - x_3)^2 + (y - y_3)^2 + (z - z_3)^2 = [v \times (T_1 + \tau_{31})]^2 \quad [3]$$

$$(x - x_4)^2 + (y - y_4)^2 + (z - z_4)^2 = [v \times (T_1 + \tau_{41})]^2 \quad [4]$$

Experimental Setup

A laboratory-based experiment was set up for UHF PD signal acquisition in accordance with IEC 60270 and IEC TS 62478 (Hashim et al., 2023), as illustrated in Figure 2. The test tank used in the setup was made of steel, with 4 side walls 1 mm thick. A total of 65 litres of mineral oil, with a viscosity of 9.6 mm^2/s at 40°C and a density of 0.875 kg/dm^3 at 20°C, was filtered and dried based on the procedures outlined in (Hashim et al., 2023; Mohd Hashim et al., 2023). The treated oil was then transferred into the test tank. A needle with a tip radius of 3 μm and a copper plane electrode with a diameter of 50 mm and an edge radius of 3 mm were used to establish a needle-to-plane electrode configuration (Hashim et al., 2023). The electrode configuration was placed at 2 distinct locations within the test

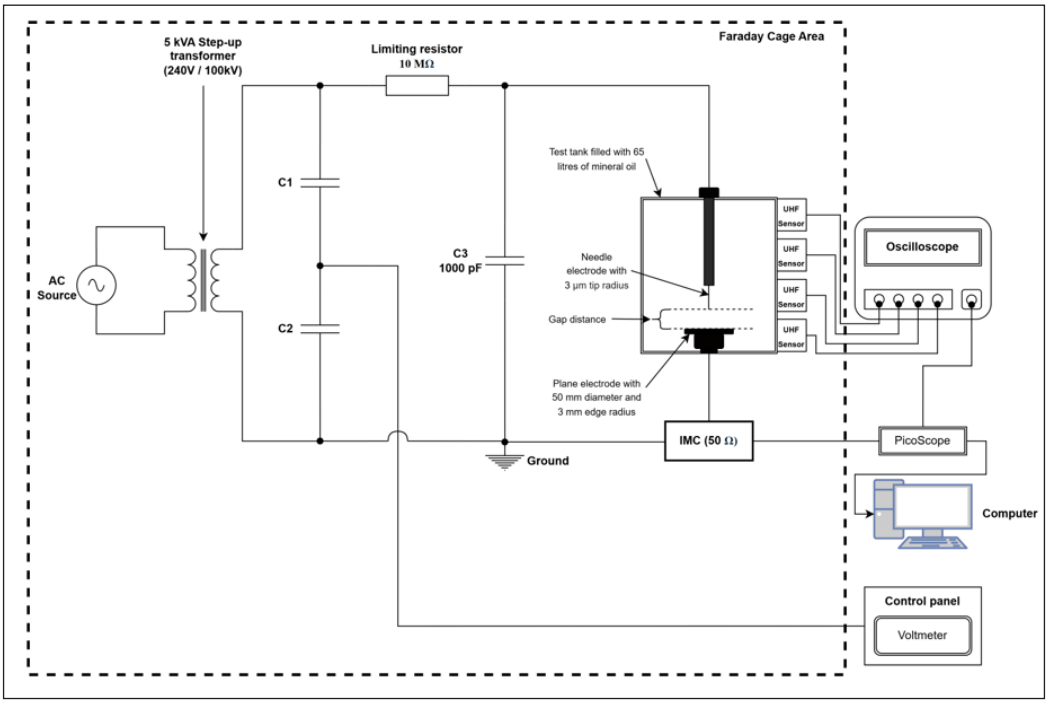

Figure 2. Experimental setup for UHF PD signal acquisition

tank, one at a time, to create 2 PD source locations. Based on the coordinate system depicted in Figure 1, the tip of the needle electrode was positioned at (0.500, 0.150, 0.080) m for PD Location 1 and (0.250, 0.100, 0.083) m for PD Location 2. The gap distances between the needle and plane electrodes for the 2 PD locations were fixed at 35 mm and 38 mm, respectively. In total, 4 patch-type wideband antennas with a frequency range of 0.7 to 2.7 GHz served as the UHF sensors and were connected to a LeCroy WaveMaster 830Zi oscilloscope to capture the UHF PD signals emitted by the PD source. The oscilloscope's measurement bandwidth and sampling rate were set to 3 GHz and 40 GS/s, respectively (Sinaga et al., 2012). At the same time, an impedance matching circuit (IMC) with 50 Ω input and output impedances, along with a PicoScope 6804E, was used to perform electrical PD measurements. These electrical PD signals were used to verify the occurrence of PD and were excluded from further analysis. A total of 20 random combinations of sensor coordinates were used to acquire UHF PD signals at each PD location. Each combination comprised the coordinates of the 4 UHF sensors positioned at different locations on the 4 side walls of the test tank.

UHF PD Signal Denoising and TDOA Computation

The VMD algorithm was applied in accordance with Long et al. (2017) and Zhang et al. (2019) to denoise the UHF PD signals obtained from the experiment. The quadratic penalty term, α, and the time-step of the dual ascent, τ, were set to 2,000 and 0, respectively (Zhang et al., 2019). Each of the UHF PD signals was decomposed into several band-limited intrinsic mode functions (BLIMFs), which are amplitude-modulated and frequency-modulated signal components within specific frequency bands (Zhang et al., 2019). The total bandwidth of the BLIMFs was minimised while the sum of all BLIMFs exactly reproduced the original PD signal. The number of decomposition modes in the VMD, K, was adaptively selected based on the mode-mixing judgement algorithm proposed by Zhang et al. (2019). Initially, K was set to 2 and increased by 1 if the frequency spectrum of any BLIMF contained more than one active component. To avoid excessive computation time, the maximum K was limited to 10. The segmentation length of the frequency spectrum, L_1, and the threshold for amplitude criterion, g, in the mode-mixing judgement algorithm were set to 10,000 and 0.5, respectively (Zhang et al., 2019). Equation 5 was employed to calculate the kurtosis of each of the BLIMFs (Zhang et al., 2019), where X represents the BLIMF, $x(i)$ denotes the ith sample of the BLIMF, $\bar{x}$ is the mean of the BLIMF, and n is the total number of samples in the BLIMF. The calculated kurtoses were subsequently used to identify the effective BLIMFs that contain significant PD signal components. Since kurtosis is sensitive to sudden changes in the BLIMF waveform, BLIMFs associated with PD generally exhibit higher kurtoses than the noise-dominated BLIMFs (Zhang et al., 2019). This is because UHF PD signals are characterised by transient pulses with a very short rise

time followed by damped oscillations (Zhang et al., 2019). Therefore, based on the criterion proposed by Long et al. (2017) and Zhang et al. (2019), BLIMFs with kurtoses greater than 10 were considered effective and were used to reconstruct the denoised UHF PD signal.

$$Kurtosis\ (X) = \frac{\frac{1}{n}\sum_{i=1}^{n}(x(i) - \bar{x})^4}{\left(\frac{1}{n}\sum_{i=1}^{n}(x(i) - \bar{x})^2\right)^2} \quad [5]$$

The FPM and CEM were subsequently employed to compute the TDOAs from both the original and denoised UHF PD signals. In the FPM, each UHF PD signal was first converted to its absolute amplitude and then normalised to its maximum value (Sinaga et al., 2012). A magnitude threshold of 0.3 was used in this study, and the TOA was extracted at the instant where a local peak first exceeded this threshold, as depicted in Figure 3(a). The TDOA was calculated as the TOA at the sensor of interest minus the TOA at the reference sensor, as shown in Figure 3(a). For the CEM, the cumulative energy curves of the original and denoised UHF PD signals were utilised to compute the variable *S* based on the equation provided by Kundu et al. (2009). The time at the minimum point of the resulting *S* curve was identified as the TOA of the respective UHF PD signal (Kundu et al., 2009), as illustrated in Figure 3(b). The TDOAs of the CEM were computed in the same manner as in the FPM.

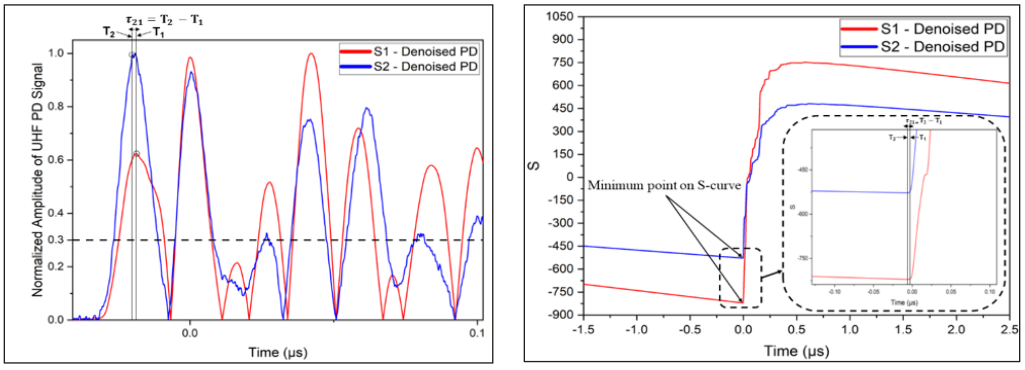

(a) (b)

Figure 3. TDOA determination based on (a) FPM and (b) CEM

Artificial Neural Networks (ANNs) Training

The procedures used to generate the datasets for ANN training are summarised in Figure 4. First, the test tank was virtually divided into a grid with 5 mm, 2 mm, and 2 mm spacing along the *x*-, *y*-, and *z*- axes, respectively. This grid resulted in a total of 3,824,226 possible

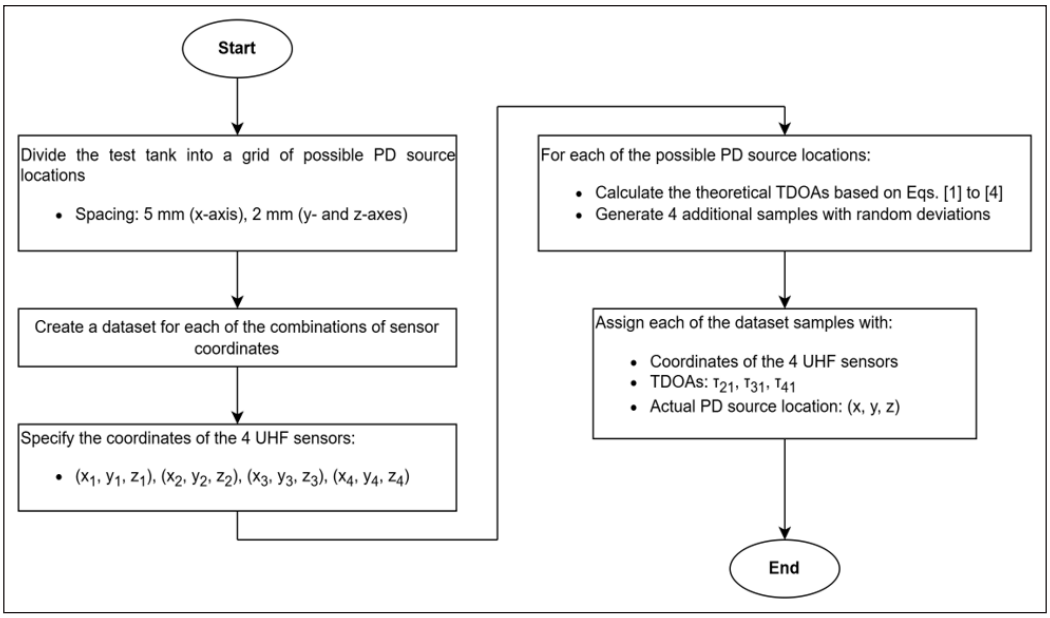

Figure 4. The dataset generation procedures based on the TDOA equations

PD source locations, as illustrated in Figure 5. For each possible PD source location, the theoretical TDOAs were calculated using Equations 1-4 to form 1 sample in the dataset. To account for factors that could affect the precise determination of TDOAs, such as the sophisticated propagation path within the transformer tank, noise at the measurement site, and other uncertainties (Ghosh et al., 2017; Jangjoo et al., 2023), 4 additional samples were created for each of the possible PD source locations. Each additional sample was generated by adding random deviations, drawn from a normal distribution with a mean of 0 ns and a standard deviation of 0.3 ns, to the theoretical TDOAs. This approach aligns with Zaki et al. (2020), who reported that TDOA determination errors can be modelled with a normal distribution. These steps were repeated for each sensor coordinate combination considered in this study, yielding a total of 20 datasets.

The adaptive moment estimation (Adam) algorithm was employed to train the ANNs (Kingma & Ba, 2014), with the maximum number of epochs capped at 300 and the mini-batch size set to 1,912,113 samples. The initial learning rate, η, the exponential decay rate for the first moment, β_1, and the exponential decay rate for the second moment, β_2, were set to 0.001, 0.9, and 0.999, respectively (Kingma & Ba, 2014). The architecture of the ANNs was determined by the steps shown in Figure 6. The training inputs were normalised by a constant of 5.37 ns, which represents the theoretical maximum TDOA within the test tank. This constant was obtained by dividing the tank diagonal length by the propagation velocity of UHF PD signals in oil. For each of the hidden layers, the smallest number of

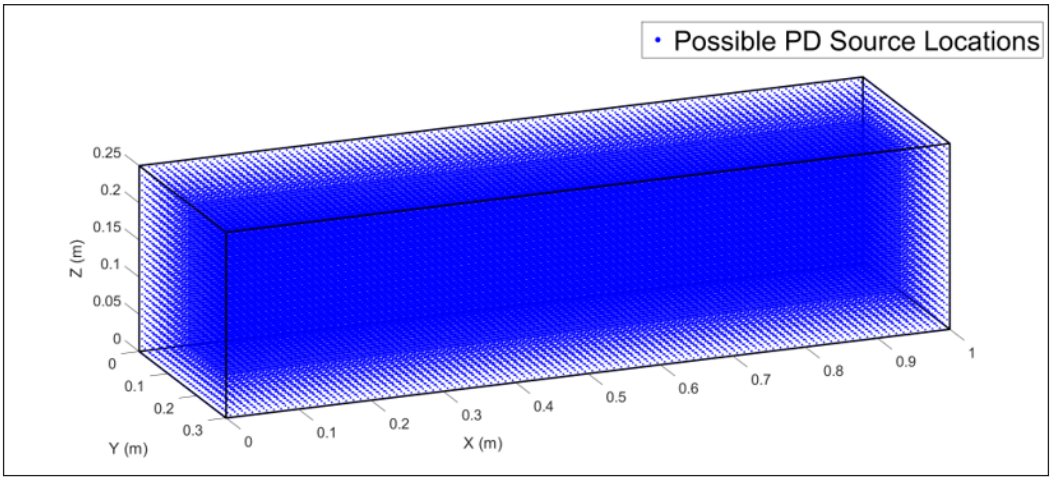

Figure 5. The virtual grid of possible PD source locations within the test tank

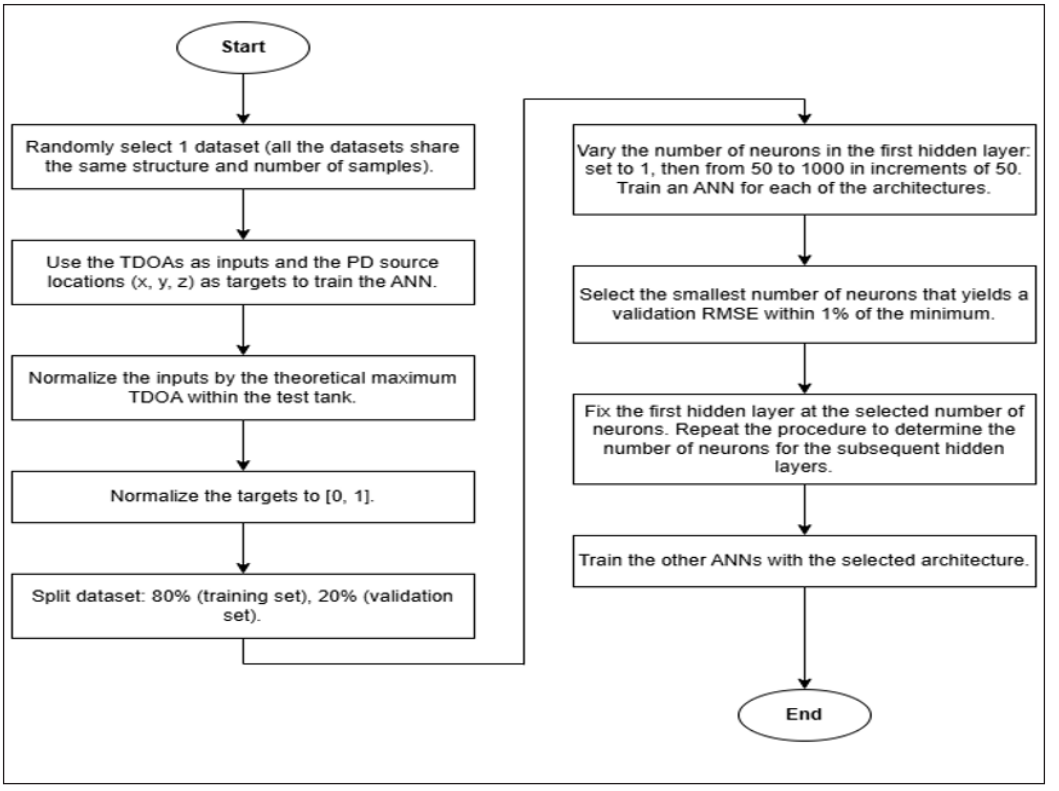

Figure 6. The steps used to determine the architecture for the ANNs in this study

neurons that produced a validation RMSE no more than 1% above the minimum RMSE was selected. For instance, the minimum RMSE was achieved by 1,000 neurons in the first hidden layer, at 0.10. However, the number of neurons in the first hidden layer was set to 600 because this configuration resulted in a 24.02% shorter training time with only a 0.99% higher RMSE, as depicted in Figure 7.

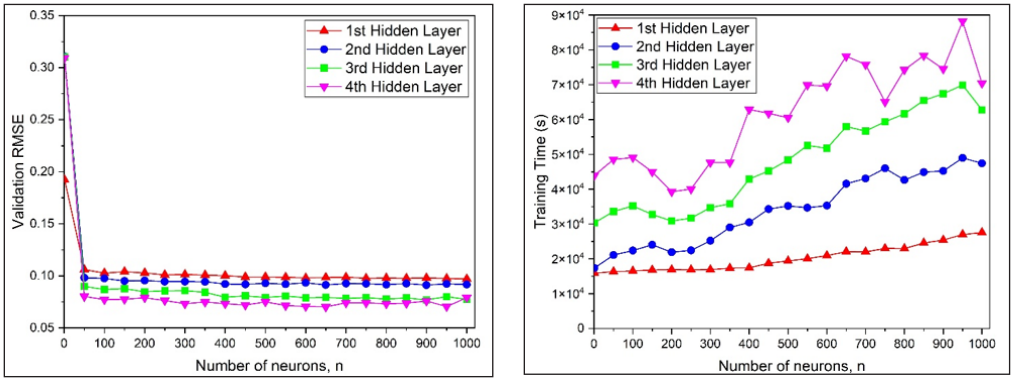

(a) (b)

Figure 7. (a) Validation RMSE and (b) training time for all the tested ANN architectures

According to the steps in Figure 6, the selected ANN architecture comprised 3 hidden layers with 600, 400, and 400 neurons, respectively, as illustrated in Figure 8. The rectified linear unit (ReLU) activation function was applied to all the hidden-layer neurons (Khodaveisi et al., 2024). For PD localisation, each of the ANNs was configured with 3 input neurons for the TDOAs and 3 output neurons for the *x*-, *y*-, and *z*- coordinates of the estimated PD location. As indicated in Figure 7, the architecture was chosen to balance ANN performance and training time. Thus, it may not represent the optimal design. The validation set performance of the trained ANNs was assessed by the root mean square error (RMSE) and Pearson correlation coefficients (R_x, R_y, R_z) given in Equations 6, 7a, 7b and 7c (Khodaveisi et al., 2024). In these equations, the predicted PD location for the ith validation sample was expressed as $(x_{p,i}, y_{p,i}, z_{p,i})$, while the corresponding actual PD location was denoted by $(x_{c,i}, y_{c,i}, z_{c,i})$. The terms $\overline{x_p}$, $\overline{y_p}$, and $\overline{z_p}$ represented the mean of the predicted PD source coordinates, whereas $\overline{x_c}$, $\overline{y_c}$, and $\overline{z_c}$ denoted the mean of the actual PD source coordinates, computed across *n* samples, where *n* is the total number of validation samples.

$$RMSE = \sqrt{\frac{1}{n}\sum_{i=1}^{n}\left[\left(x_{p,i} - x_{c,i}\right)^2 + \left(y_{p,i} - y_{c,i}\right)^2 + \left(z_{p,i} - z_{c,i}\right)^2\right]} \qquad [6]$$

$$R_x = \frac{\sum_{i=1}^{n}(x_{p,i}-\overline{x_p})(x_{c,i}-\overline{x_c})}{\sqrt{\left[\sum_{i=1}^{n}(x_{p,i}-\overline{x_p})^2\right]\left[\sum_{i=1}^{n}(x_{c,i}-\overline{x_c})^2\right]}} \quad [7a]$$

$$R_y = \frac{\sum_{i=1}^{n}(y_{p,i}-\overline{y_p})(y_{c,i}-\overline{y_c})}{\sqrt{\left[\sum_{i=1}^{n}(y_{p,i}-\overline{y_p})^2\right]\left[\sum_{i=1}^{n}(y_{c,i}-\overline{y_c})^2\right]}} \quad [7b]$$

$$R_z = \frac{\sum_{i=1}^{n}(z_{p,i}-\overline{z_p})(z_{c,i}-\overline{z_c})}{\sqrt{\left[\sum_{i=1}^{n}(z_{p,i}-\overline{z_p})^2\right]\left[\sum_{i=1}^{n}(z_{c,i}-\overline{z_c})^2\right]}} \quad [7c]$$

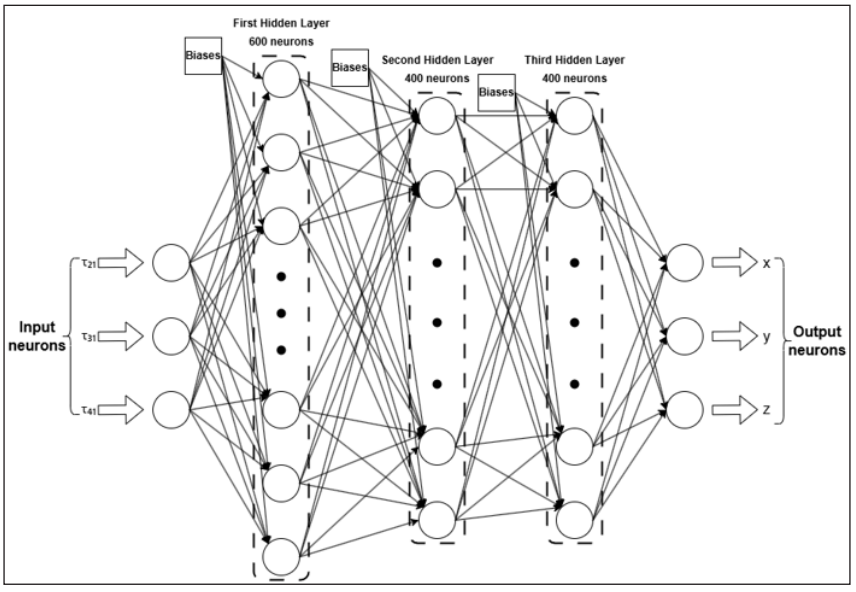

Figure 8. The ANN architecture used in this study

PD Localisation Performance Analysis

The 4 TDOA scenarios derived from the experimental UHF PD signals were used to evaluate the PD localisation performance of the trained ANNs. For simplicity, the TDOAs computed from the original UHF PD signals through the FPM and CEM were referred to as Scenarios 1 and 2, respectively, whereas the TDOAs computed from the denoised UHF PD signals through the FPM and CEM were designated as Scenarios 3 and 4, respectively. The artificial bee colony (ABC) (Lim et al., 2025), bat algorithm (BA) (Chakravarthi et al., 2017), genetic algorithm (GA) (Cintra Veloso et al., 2006), particle swarm optimisation (PSO) (Tang et al., 2008), which are optimisation algorithms, along with the non-iterative algorithm proposed by Kundu et al. (2009), were employed to benchmark the PD

localisation performance of the ANNs. The parameters and implementation procedures of the optimisation algorithms were adopted from Lim et al. (2025). Equation 8 was used to calculate the distance error between the estimated and actual PD locations (Desai & Sarathi, 2018; Lim et al., 2025). The average distance error was computed as the mean across all combinations of sensor coordinates for each PD location. The average computation time for each PD localisation algorithm was also recorded for comparison.

$$\Delta D = \sqrt{(x_{actual} - x_{estimated})^2 + (y_{actual} - y_{estimated})^2 + (z_{actual} - z_{estimated})^2} \quad [8]$$

RESULTS AND DISCUSSION

UHF PD Signal Acquisition and VMD Denoising

An example of the electrical and UHF PD signals obtained from the experiment is shown in Figure 9. A slight time delay of a few nanoseconds (ns) is observed between the first peaks of the UHF PD signals and the first peak of the electrical PD signal. This delay is likely due to the propagation of the PD signals as electromagnetic waves from the PD source to the UHF sensors. Electrical PD measurements are carried out with a calibrated IMC, where an apparent charge of 100 pC corresponds to an output voltage of 258 mV ± 20 mV. The electrical pulse in Figure 9 exceeds this voltage level and is therefore identified as a PD pulse. The close alignment between the electrical and UHF pulses suggests that both signals originate from the same source and therefore supports the identification of the UHF pulses as PD signals.

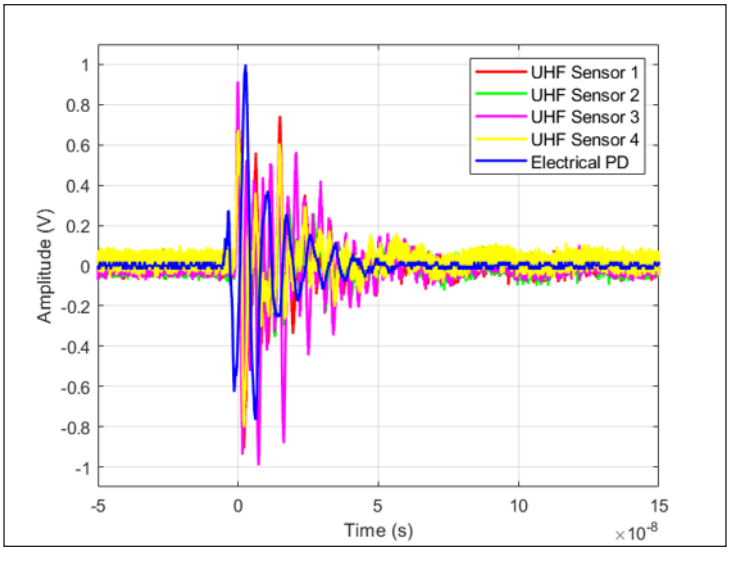

Figure 9. An example of the electrical and UHF PD signals obtained from the experiment

The effect of VMD denoising on the UHF PD signal is illustrated in Figure 10(a), where the magnitude of the PD signal is slightly reduced, while the general shape of the PD pulse is retained. VMD denoising also smooths the PD waveform and reduces ripples, as shown in Figure 10(a). Figure 10(b) depicts an example of the decomposition of an original UHF PD signal into 7 BLIMFs based on the VMD and mode-mixing judgment algorithm. It is observed that only the 7th BLIMF has a kurtosis greater than 10. Therefore, it is considered the effective BLIMF and is used to reconstruct the denoised UHF PD signal. Based on the equations in Mohd Hashim et al. (2023), the average normalised correlation coefficient (NCC) and the normalised root mean square error (NRMSE) between the original and denoised UHF PD signals at PD Location 1 are 0.91 and 0.40, respectively. For PD Location 2, the average NCC is 0.86, and the average NRMSE is 0.50. The average time required to denoise the UHF PD signals is 126.8 s for PD Location 1 and 96.1 s for PD Location 2.

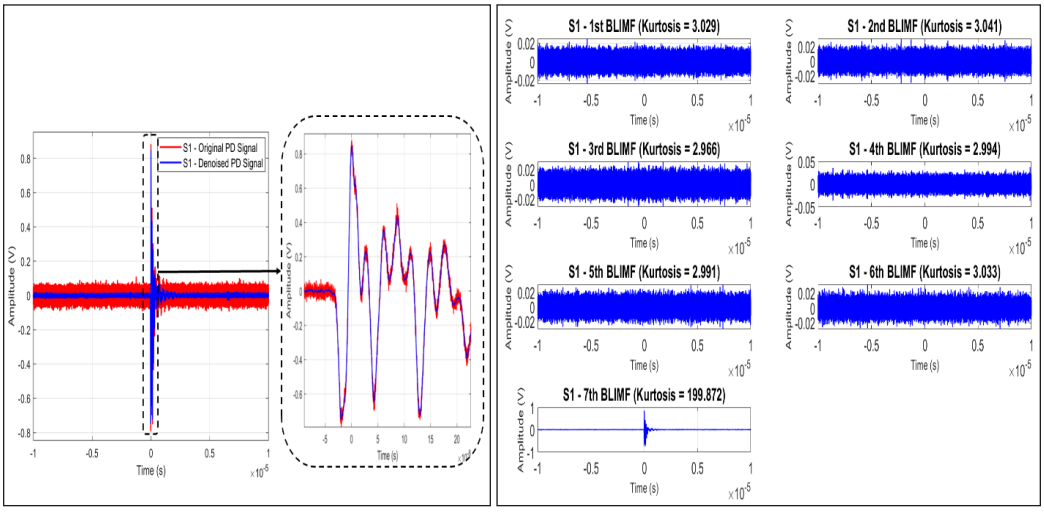

(a) (b)

Figure 10. (a) Example of original and denoised UHF PD signals. (b) BLIMFs obtained from the decomposition of the original UHF PD signal in (a)

TDOA Computation Based on FPM and CEM

Figure 11(a) shows the mean absolute errors (MAEs) of the TDOAs derived from the UHF PD signals of PD Location 1. The MAEs are computed in 2 steps. First, the absolute differences between the TDOAs derived from the original or denoised UHF PD signals and the theoretical TDOAs computed from Equations 1-4 are calculated. Second, the absolute differences across all combinations of sensor coordinates are averaged to obtain the MAEs. For PD Location 1, the τ_{21}, τ_{31}, and τ_{41} in Scenario 1 have MAEs that are 26.01%, 24.45%, and 30.01% lower than those in Scenario 2, while the MAEs in Scenario

4 are 47.11%, 49.15%, and 52.68% lower than those in Scenario 3. As illustrated in Figure 11(b), a similar trend is observed for PD Location 2, where Scenario 1 yields 30.29%, 29.26%, and 23.69% lower MAEs than Scenario 2, and Scenario 4 produces 44.58%, 44.25%, and 46.39% lower MAEs than Scenario 3. These findings indicate that neither the FPM nor the CEM consistently outperforms the other. The FPM yields lower MAEs for the original UHF PD signals, whereas the CEM produces lower MAEs for the denoised UHF PD signals. In addition, VMD denoising improves the UHF PD signal waveforms and enables both the FPM and the CEM to achieve lower MAEs in TDOA computation.

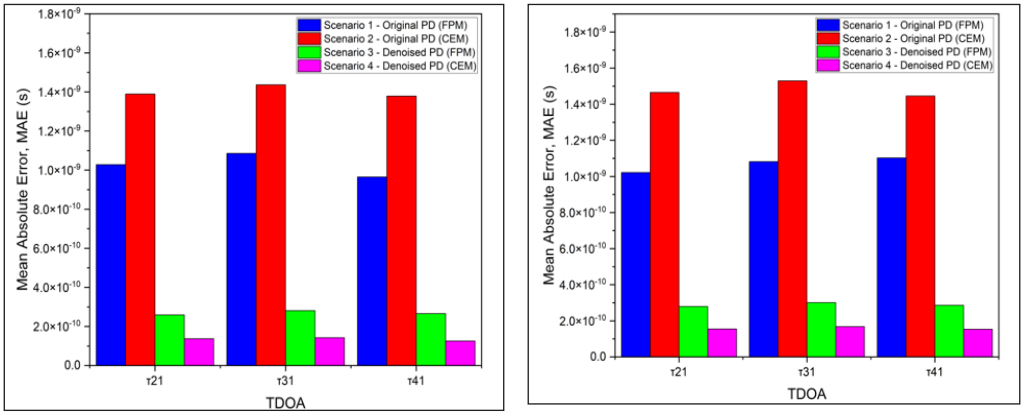

Figure 11. Mean absolute errors of the TDOAs obtained by the FPM and CEM from the original and denoised UHF PD signals of (a) PD Location 1 and (b) PD Location 2

Validation Set Performance of the Trained ANNs

In this study, validation sets are used instead of independent test sets because the trained ANNs are subsequently evaluated using the TDOAs derived from the experimental UHF PD signals. Figure 12 depicts the validation RMSE and the Pearson correlation coefficients of all 20 trained ANNs. It is found that the correlation R_x is the highest, ranging from 0.96 to 0.99. This indicates that the x-coordinates predicted by the ANNs are very close to the target x-coordinates. The correlations R_y and R_z are lower, with an average of 0.88 and 0.74, respectively. The weak performance along the y- and z-axes is likely due to the shorter dimensions of the test tank in these directions (Khodaveisi et al., 2024), which leads to less variation in the corresponding coordinates among the samples in the datasets. The trained ANNs achieve an average RMSE of 7.23 cm, which is comparable to the performance reported for the backpropagation neural network in Khodaveisi et al. (2024).

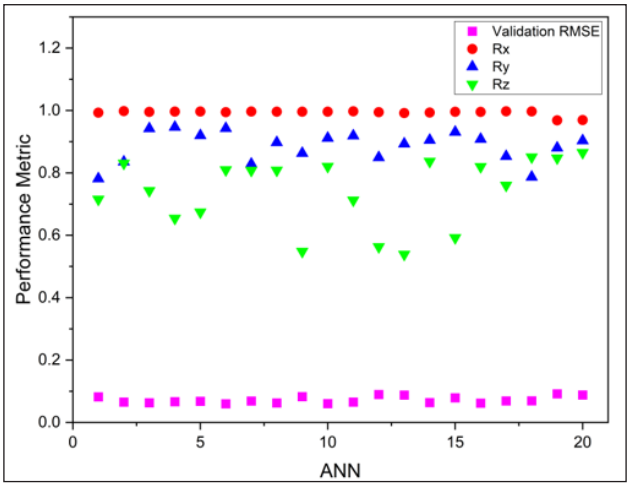

Figure 12. Validation RMSE and Pearson correlation coefficients of the trained ANNs

PD Localisation Performance Analysis

The estimated PD locations produced by the trained ANNs, ABC, BA, GA, PSO, and the non-iterative algorithm for PD Location 1 are presented in Figure 13. Figure 14(a) shows that the PD localisation algorithms yield lower average distance errors in Scenario 1 than in Scenario 2. The distance errors decrease when the UHF PD signals are denoised, as indicated by Scenarios 3 and 4. Scenario 4 produces lower distance errors than Scenario 3. These results demonstrate that PD localisation accuracy is affected by the precision of TDOA computation (Chan et al., 2023; Desai & Sarathi, 2018), where TDOAs with low MAEs lead to high PD localisation accuracy. As shown in Figure 14(a), the trained ANNs achieve the highest PD localisation accuracy across all 4 scenarios. For instance, in Scenario 4, the trained ANNs record the lowest average distance error of 5.74 cm, which is 46.34%, 46.59%, 49.83%, 49.77%, and 56.60% lower than the errors of the ABC, BA, GA, PSO, and the non-iterative algorithm, respectively. In contrast, the non-iterative algorithm consistently produces the lowest localisation accuracy because a few of its estimated PD locations fall outside the tank, as illustrated in Figure 13. When both solutions from the non-iterative algorithm are located outside the tank, the one closest to the actual PD location is taken as the estimated PD location. However, some of the out-of-tank estimated PD locations are too far and are thus not displayed in Figure 13. The ABC, BA, GA, and PSO algorithms exhibit similar PD localisation accuracy across the 4 scenarios. However, as depicted in Figure 14(b), the ABC algorithm has the shortest average computation time. The trained ANNs require 37.97 to 43.17 ms to estimate the PD locations, whereas all the optimisation algorithms have average computation times above 638 ms. The non-iterative algorithm provides the fastest PD localisation, with an average computation time of 0.34 to 0.57 ms.

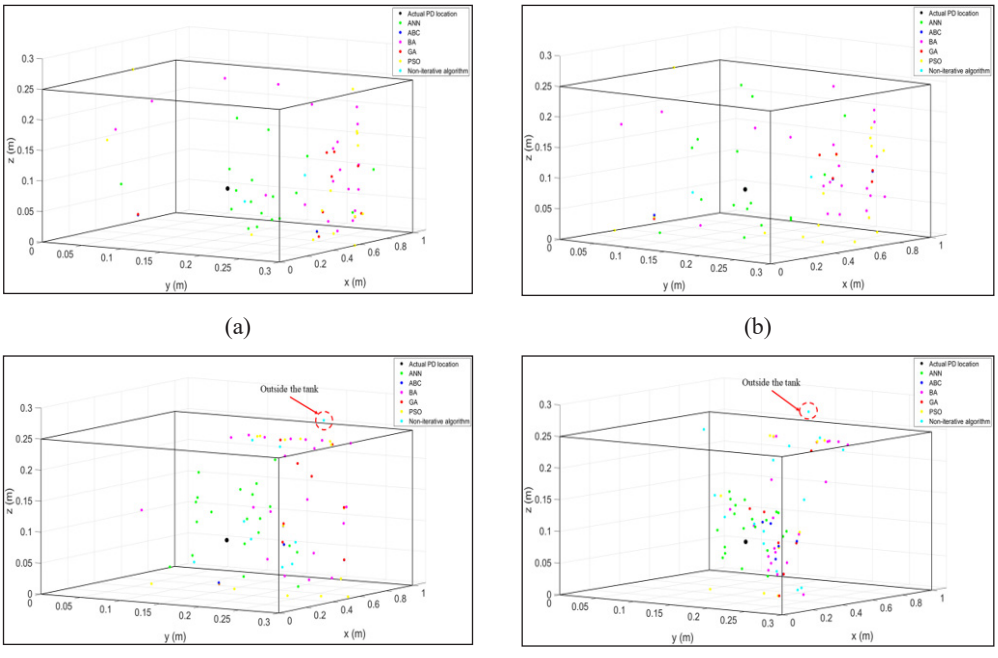

Figure 13. PD localisation results of the trained ANNs (green), ABC (blue), BA (magenta), GA (red), PSO (yellow), and the non-iterative algorithm (cyan) for PD Location 1 under (a) Scenario 1, (b) Scenario 2, (c) Scenario 3, and (d) Scenario 4

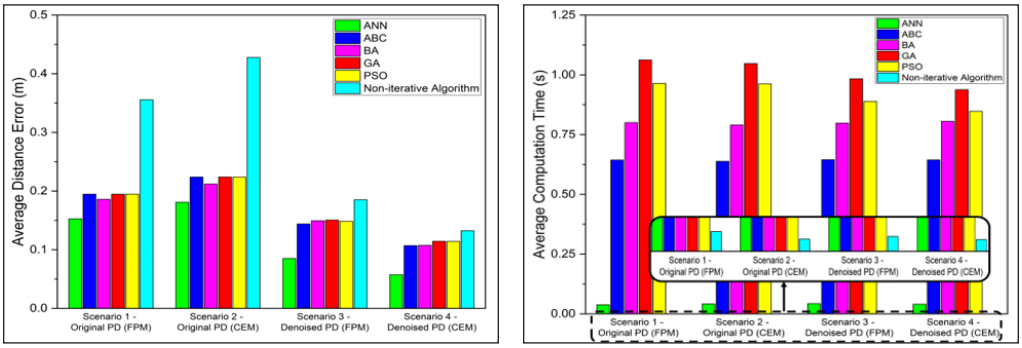

Figure 14. (a) Average distance error and (b) average computation time of the trained ANNs, ABC, BA, GA, PSO, and non-iterative algorithm for PD localisation at PD Location 1

Figure 15 illustrates the estimated PD locations obtained by the trained ANNs, ABC, BA, GA, PSO, and the non-iterative algorithm for PD Location 2. The average distance errors and average computation times for each PD localisation algorithm are presented in Figures 16(a) and 16(b), respectively. A similar trend to PD Location 1 is observed

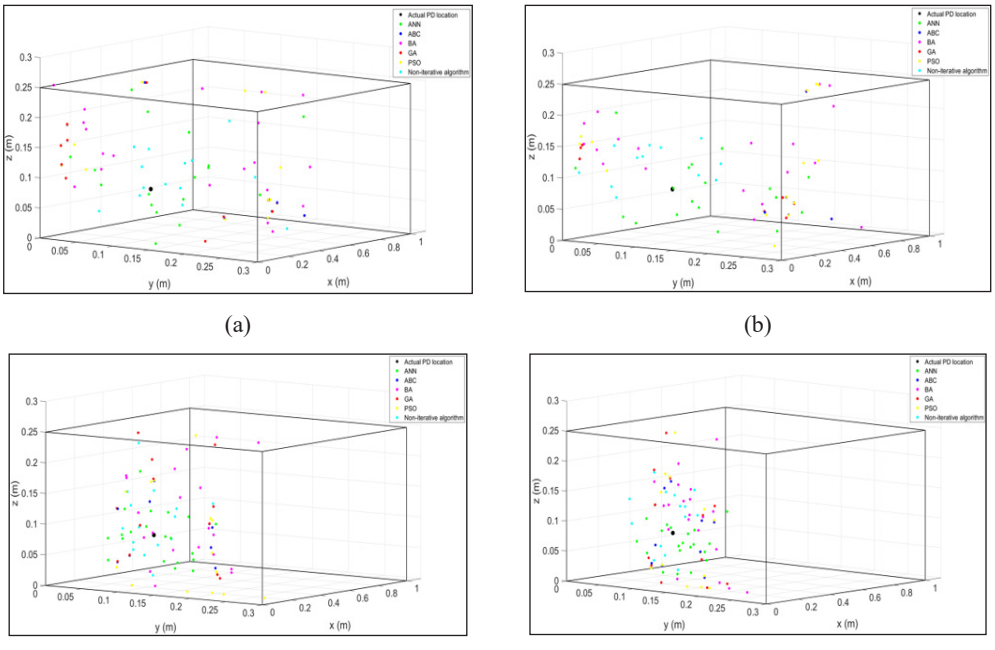

Figure 15. PD localisation results of the trained ANNs (green), ABC (blue), BA (magenta), GA (red), PSO (yellow), and the non-iterative algorithm (cyan) for PD Location 2 under (a) Scenario 1, (b) Scenario 2, (c) Scenario 3, and (d) Scenario 4

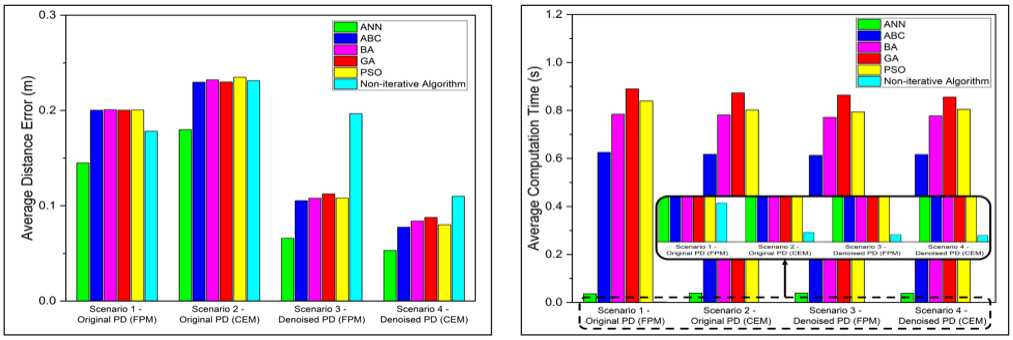

Figure 16. (a) Average distance error and (b) average computation time of the trained ANNs, ABC, BA, GA, PSO, and non-iterative algorithm for PD localisation at PD Location 2

in Figure 16(a), where Scenario 1 results in lower distance errors than Scenario 2, and Scenario 4 yields lower errors than Scenario 3. The trained ANNs produce the lowest average distance errors across all scenarios, with a minimum error of 5.32 cm in Scenario 4. This is 31.46%, 36.71%, 39.44%, 33.63%, and 51.69% lower than the errors of the ABC, BA, GA, PSO, and the non-iterative algorithm, respectively. The ABC consistently

yields higher PD localisation accuracy than the BA, GA, and PSO, as shown in Figure 16(a). For example, in Scenario 3, the distance error of the ABC is 10.54 cm, which is 2.36%, 6.33%, and 2.52% lower than the errors of the BA, GA, and PSO, respectively. In Scenario 1, the non-iterative algorithm achieves higher PD localisation accuracy than the optimisation algorithms, with an 11% lower distance error than ABC, as shown in Figure 16(a). In contrast, the non-iterative algorithm yields the largest distance errors in Scenarios 3 and 4. As depicted in Figure 16(b), the trained ANNs require an average of 36.75 to 39.71 ms to perform PD localisation for PD Location 2. This is shorter than the computation times of the optimisation algorithms, which generally exceed 613 ms. As in the case of PD Location 1, the non-iterative algorithm achieves the shortest average computation time, ranging from 0.36 ms to 2.18 ms.

Overall, the accuracy of PD localisation depends on the precision of TDOA computation. For both PD locations, TDOAs with low MAEs, obtained from the FPM for the original UHF PD signals and from the CEM for the denoised UHF PD signals, generally result in low average distance errors. The trained ANNs achieve the highest PD localisation accuracy, with minimum average distance errors of 5.74 cm and 5.32 cm for PD Locations 1 and 2, respectively. These errors correspond to 5.35% and 4.96% of the tank diagonal length, respectively. The good PD localisation accuracy of the ANNs is likely due to the datasets used for training. Random deviations are added to the theoretical TDOAs during dataset generation. As a result, the ANNs are exposed to non-ideal TDOAs during training. In contrast, the optimisation algorithms and the non-iterative algorithm do not undergo a training process prior to PD localisation. Therefore, these algorithms are more sensitive to TDOA errors compared to the trained ANNs. In terms of computation time, the trained ANNs provide faster estimations than the ABC, BA, GA, and PSO, but are slower than the non-iterative algorithm.

CONCLUSION

In conclusion, this study investigated the PD localisation performance of ANNs trained with TDOA datasets generated from the TDOA equations. The trained ANNs exhibit higher correlation for the x-coordinates as compared to the y- and z-coordinates. For the original UHF PD signals obtained from the experiment, the FPM computes the TDOAs with lower MAEs than the CEM, whereas for the UHF PD signals denoised by the VMD method, the CEM records lower MAEs than the FPM. The PD localisation results indicate that TDOAs with low MAEs generally yield lower average distance errors. For all PD locations and TDOA scenarios in this study, PD localisation with the trained ANNs consistently yields the lowest average distance errors. This suggests that the dataset generation procedures adopted in this study offer an alternative to extensive field data collection or simulation-based approaches. The average computation time of the trained ANNs for UHF PD

localisation is shorter than that of the ABC, BA, GA, and PSO, but longer than that of the non-iterative algorithm.

ACKNOWLEDGEMENT

This study was funded by Universiti Putra Malaysia Inisiatif Putra (Fast Track) (GP-FASTRACK/2024/9791100) funding scheme and Inisiatif Putra Berkumpulan (GP-IPB/2022/9717000).

LIST OF ABBREVIATIONS

ABC	Artificial bee colony
Adam	Adaptive moment estimation
AI	Artificial intelligence
ANFIS	Adaptive Neuro-Fuzzy Inference System
ANN	Artificial neural network
BA	Bat algorithm
BLIMF	Band-limited intrinsic mode function
BPNN	Backpropagation Neural Network
CCM	Cross-Correlation Method
CEM	Cumulative Energy Method
EMD	Empirical mode decomposition
FPM	First Peak Method
GA	Genetic algorithm
IMC	Impedance matching circuit
MAE	Mean absolute error
MW	Multivariate wavelet denoising
NCC	Normalised correlation coefficient
NRMSE	Normalised root mean square error
PD	Partial discharge
PSO	Particle swarm optimisation
QGA	Quantum genetic algorithm
ReLU	Rectified linear unit
RMSE	Root mean square error
SNR	Signal-to-noise ratio
SVM	Support vector machine
TDOA	Time Difference of Arrival
TOA	Time of arrival

UHF Ultra-high frequency
VMD Variational mode decomposition

REFERENCES

AJ, C., Salam, M. A., Rahman, Q. M., Wen, F., Ang, S. P., & Voon, W. (2018). Causes of transformer failures and diagnostic methods – a review. *Renewable and Sustainable Energy Reviews*, *82*, 1442-1456. https://doi.org/10.1016/j.rser.2017.05.165

Basheer, I. A., & Hajmeer, M. (2000). Artificial neural networks: Fundamentals, computing, design, and application. *Journal of Microbiological Methods*, *43*(1), 3-31. https://doi.org/10.1016/S0167-7012(00)00201-3

Boya-Lara, C., Rivera-Caballero, O., & Ardila-Rey, J. A. (2022). A comparative study of denoising techniques for UHF signals from partial discharge. In *2022 8th International Engineering, Sciences and Technology Conference (IESTEC)* (pp. 595-601). IEEE. https://doi.org/10.1109/IESTEC54539.2022.00099

Chakravarthi, M. K., Giridhar, A. V., & Sarma, D. V. S. S. S. (2017). Localization of partial discharge source in power transformer using bat algorithm. In *2017 7th International Conference on Power Systems (ICPS)* (pp. 382-385). IEEE. https://doi.org/10.1109/ICPES.2017.8387324

Chan, J. Q., Raymond, W. J. K., Illias, H. A., & Othman, M. (2023). Partial discharge localization techniques: A review of recent progress. *Energies*, *16*(6), Article 2863. https://doi.org/10.3390/en16062863

CIGRE Working Group D1.29 (2017). *Partial discharges in transformers (CIGRE technical brochure no. 676).* CIGRE.

Cintra Veloso, G., Borges Da Silva, L., Lambert-Torres, G., & Pinto, J. O. P. (2006). Localization of partial discharges in transformers by the analysis of the acoustic emission. In *2006 IEEE International Symposium on Industrial Electronics* (pp. 537-541). IEEE. https://doi.org/10.1109/ISIE.2006.295515

Desai, B. M. A., & Sarathi, R. (2018). Identification and localisation of incipient discharges in transformer insulation adopting UHF technique. *IEEE Transactions on Dielectrics and Electrical Insulation*, *25*(5), 1924-1931. https://doi.org/10.1109/TDEI.2018.007294

Ghosh, R., Chatterjee, B., & Dalai, S. (2017). A method for the localization of partial discharge sources using partial discharge pulse information from acoustic emissions. *IEEE Transactions on Dielectrics and Electrical Insulation*, *24*(1), 237-245. https://doi.org/10.1109/TDEI.2016.006080

Hashim, A. H. M., Azis, N., Jasni, J., Radzi, M. A. M., Kozako, M., Jamil, M. K. M., & Yaakub, Z. (2023). Application of ANFIS and ANN for partial discharge localization in oil through acoustic emission. *IEEE Transactions on Dielectrics and Electrical Insulation*, *30*(3), 1247-1254. https://doi.org/10.1109/TDEI.2023.3264958

Jahangir, H., Akbari, A., Werle, P., & Szczechowski, J. (2017). UHF PD measurements on power transformers-advantages and limitations. *IEEE Transactions on Dielectrics and Electrical Insulation*, *24*(6), 3933-3940. https://doi.org/10.1109/TDEI.2017.006149

Jangjoo, M. A., Allahbakhshi, M., & Mirzaei, H. R. (2023). UHF sensors positioning on the power transformer tank to enhance the partial discharge localization accuracy. *Electric Power Systems Research*, *218*, Article 109174. https://doi.org/10.1016/j.epsr.2023.109174

Kakeeto, P., Judd, M., Pearson, J., & Templeton, D. (2008). Experimental investigation of positional accuracy for UHF partial discharge location. In *2008 International Conference on Condition Monitoring and Diagnosis* (pp. 1070-1073). IEEE. https://doi.org/10.1109/CMD.2008.4580467

Khodaveisi, F., Karami, H., Karimpour, M. Z., Rubinstein, M., & Rachidi, F. (2024). Partial discharge localization in power transformer tanks using machine learning methods. *Scientific Reports*, *14*(1), Article 11785. https://doi.org/10.1038/s41598-024-62527-9

Kingma, D. P., & Ba, J. (2014). *Adam: A method for stochastic optimization.* arXiv. https://doi.org/10.48550/arXiv.1412.6980

Kundu, P., Kishore, N. K., & Sinha, A. K. (2009). A non-iterative partial discharge source location method for transformers employing acoustic emission techniques. *Applied Acoustics*, *70*(11-12), 1378-1383. https://doi.org/10.1016/j.apacoust.2009.07.001

Lim, Z. Y., Azis, N., Mohd Hashim, A. H., Mohd Radzi, M. A., Norsahperi, N. M. H., & Mohd Ariffin, A. (2025). Acoustic emission partial discharge localization in oil based on artificial bee colony. *Pertanika Journal of Science and Technology*, *33*(1), 241-259. https://doi.org/10.47836/pjst.33.1.11

Long, J., Wang, X., Dai, D., Tian, M., Zhu, G., & Zhang, J. (2017). Denoising of UHF PD signals based on optimised VMD and wavelet transform. *IET Science, Measurement & Technology*, *11*(6), 753-760. https://doi.org/10.1049/iet-smt.2016.0510

Long, J., Wang, X., Zhou, W., Zhang, J., Dai, D., & Zhu, G. (2021). A comprehensive review of signal processing and machine learning technologies for UHF PD detection and diagnosis (i): Preprocessing and localization approaches. *IEEE Access*, *9*, 69876-69904. https://doi.org/10.1109/ACCESS.2021.3077483

Mohd Hashim, A. H., Azis, N., Jasni, J., Mohd Radzi, M. A., Kozako, M., Mohd Jamil, M. K., & Yaakub, Z. (2023). Examination on the denoising methods for electrical and acoustic emission partial discharge signals in oil. *Indonesian Journal of Electrical Engineering and Informatics (IJEEI)*, *11*(3), 791-804. https://doi.org/10.52549/ijeei.v11i3.4463

Pattanadech, N., & Muhr, M. (2016). Partial discharge inception voltage investigation of mineral oil: Effect of electrode configurations and oil conditions. *IEEE Transactions on Dielectrics and Electrical Insulation*, *23*(5), 2917-2924. https://doi.org/10.1109/TDEI.2016.7736853

Rathod, V. B., Kumbhar, G. B., & Bhalja, B. R. (2022). Partial discharge detection and localization in power transformers based on acoustic emission: Theory, methods, and recent trends. *IETE Technical Review*, *39*(3), 540-552. https://doi.org/10.1080/02564602.2021.1871672

Sinaga, H. H., Phung, B. T., & Blackburn, T. R. (2012). Partial discharge localization in transformers using UHF detection method. *IEEE Transactions on Dielectrics and Electrical Insulation*, *19*(6), 1891-1900. https://doi.org/10.1109/TDEI.2012.6396945

Taha, I. B. M., Dessouky, S. S., Ghaly, R. N. R., & Ghoneim, S. S. M. (2020). Enhanced partial discharge location determination for transformer insulating oils considering allocations and uncertainties of

acoustic measurements. *Alexandria Engineering Journal*, *59*(6), 4759-4769. https://doi.org/10.1016/j.aej.2020.08.041

Tang, L., Luo, R., Deng, M., & Su, J. (2008). Study of partial discharge localization using ultrasonics in power transformer based on particle swarm optimization. *IEEE Transactions on Dielectrics and Electrical Insulation*, *15*(2), 492-495. https://doi.org/10.1109/TDEI.2008.4483469

Zaki, A. U. M., Hu, Y., & Jiang, X. (2020). Partial discharge localization in 3-D with a multi-dnn model based on a virtual measurement method. *IEEE Access*, *8*, 87434-87445. https://doi.org/10.1109/ACCESS.2020.2993190

Zhang, J., He, J., Long, J., Yao, M., & Zhou, W. (2019). A new denoising method for UHF PD signals using adaptive VMD and SSA-Based shrinkage method. *Sensors*, *19*(7), Article 1594. https://doi.org/10.3390/s19071594